Accurate DoA Estimation Based on 1-Bit Amplitude-Adjustable Metasurface With Spatio-Temporal Modulation

Bin Zheng, Xiaofei Jiang, Kaiyin Yu, Lin Li, Chuandong Yu, Na Li, and Yiqun Zhang

***Abstract*—In this letter, we propose a transmissive amplitude-adjustable metasurface designed to achieve precise single-channel direction of arrival (DoA) estimation. Unlike most phase-controllable metasurfaces, the proposed metasurface enables amplitude controllability by integrating diodes within each unit. Furthermore, harmonics are generated based on the principle of spatiotemporal modulation for angle estimation. Additionally, the subwavelength characteristics of the metasurface units contribute to their miniaturization feature. Simulation and experimental results demonstrate that a 6 × 6 metasurface can attain high-precision DoA estimation with an accuracy of less than 0.61° within a range from 0° to 60°. The adjustable amplitude direction-finding system offers accuracy in a low-profile, compact design with a simple structure, making it suitable for uncrewed aircraft, radar, and satellite communication applications.**

***Index Terms*—Amplitude-adjustable metasurface, direction of arrival (DoA) estimation, spatio-temporal modulation.**

I. Introduction

In RECENT years, direction-of-arrival (DoA) estimation or direction finding has assumed a critical role in contemporary signal processing research due to the rapid advancement of 6G communication systems and the burgeoning low-altitude economy [1], [2]. This technology enables the detection of the propagation direction of electromagnetic waves (EM), thereby facilitating the localization and tracking of target sources. This technological breakthrough has enabled widespread deployment across strategic domains such as autonomous driving, radar detection, and uncrewed aerial vehicle (UAV) applications [3], [4], [5]. The traditional direction-finding system includes antenna arrays, radio frequency devices, and signal processing modules, which cause limitations, such as high hardware complexity, cost, and power consumption [6], [7], [8].

In the 1960s, the time-modulated array (TMA) concept was introduced to synthesize the ultralow sidelobe level pattern [9]. In 2014, the feasibility of direction-finding methods based on binary TMA was first validated by establishing a rigorous mathematical relationship for harmonic components to determine the incident angle [10]. Since then, the direction-finding method based on TMA has flourished [11], [12], [13]. Compared to conventional direction-finding methods, TMA introduces high-speed switches at the front end of traditional antenna arrays, achieving relatively low hardware and computational complexities [14], [15]. Although TMA-based direction-finding technology saves on radio frequency devices and offers certain advantages, the multiantenna array still faces high cost, large size, spectrum leakage from high-speed switching reliance, and poor direction-finding accuracy [16], [17].

Meanwhile, metasurfaces, particularly spatio-temporal modulation metasurfaces (STMM) integrated with tuning devices, have garnered significant attention from researchers across various disciplines [18], [19], [20]. This interest stems from their remarkable electromagnetic properties, which allow for the manipulation of phase [18], amplitude [19], and polarization [20]. In particular, by elaborately designing the spatio-temporal coding matrix, STMM can achieve flexible spatial modulation of EM waves by controlling the diode state through a field-programmable gate array (FPGA). This configuration allows for DoA estimation using a single receiver, greatly simplifying the system structure.

Recently, several DoA estimations based on metasurfaces have been proposed [21], [22], [23], [24]. Lin et al. [25] use STMM to generate random radiation maps to perceive the incident signal and conduct DoA estimation. In [26], a random double-beam approach is employed to generate the sensing matrix and sample the incident wave, improving the limitations of entirely random radiation patterns that discrete errors can influence. Zhou et al. [27] modulate the incident wave on a time-domain orthogonal encoded metasurface to estimate DoA based on the amplitude and phase distribution of the received signal. However, these works assume that the reflection amplitudes of the metasurface in the two states are the same, mainly achieving the tuning performance between state 0 and 1 through phase responses of 0° and 180°. Research on achieving DoA estimation through the modulation of transmission amplitude in metasurfaces remains relatively scarce. Subsequently, Xia et al. [28] propose a method based on amplifier-integrated active metasurfaces specifically for single-channel systems. This method of regulating amplitude significantly enhances the accuracy of system estimation; however, the incorporation of an active amplifier also adds complexity to the overall structure.

In this work, we designed an STMM based on amplitude-adjustable elements for DoA estimation. This configuration retains the advantages of single-channel reception while offering the benefits of low cost, a simple structure, and high estimation accuracy.

Received 30 September 2025; accepted 24 October 2025. Date of publication 4 November 2025; date of current version 5 February 2026. This work was supported by the Fundamental Research Funds for the Central Universities under Grant 20101258409, in part by the National Natural Science Foundation of China under Grant 52375262, and in part by the Shaanxi Provincial Fund for Outstanding Young Scientists under Grant 2024JC-JCQN-46. *(Corresponding author: Na Li.)*

The authors are with the State Key Laboratory of Electromechanical Coupling Technology in Electronic Equipment, Xidian University, Xi'an 710071, China (e-mail: lina@mail.xidian.edu.cn).

Digital Object Identifier 10.1109/LAWP.2025.3628338

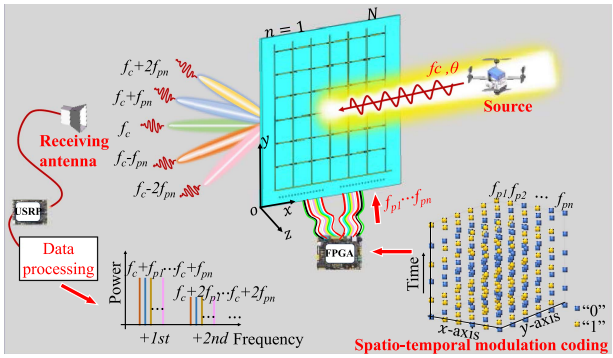

Fig. 1. Schematic diagram of the basic principle and hardware composition for DoA estimation based on STMM.

II. STMM Design and DoA Estimation Principle

This section discusses the principle and hardware composition of DoA estimation using STMM. As shown in Fig. 1, the FPGA periodically controls the diodes within the metasurface unit according to a pre-designed spatiotemporal coding sequence. When an incident signal passes through the metasurface, it generates a transmitted wave with a fundamental frequency and various harmonics. We established a spatio-temporal modulation model for the received signal and employed the MULti-SIgnal Classification (MUSIC) algorithm for DoA restoration through spatial spectrum estimation.

A. Basic Theory of STMM and 1-D DoA Estimation

As shown in Fig. 1, we propose a transmissive metasurface in which all the elements are divided into N subarrays, arranged isotropically and equally spaced. EM waves incident on the metasurface at a frequency f_c can be expressed as

$$s(t) = e^{j2\pi f_c t}. \tag{1}$$

The signal received by the subarrays can be expressed as

$$x_n(t) = \sum_{n=1}^{N} s(t) e^{-j\beta(n-1)d\sin\theta} + n(t) \tag{2}$$

Where $A = e^{-j\beta(n-1)d\sin\theta}$ is the phase information added through the nth subarray. d is the spacing between two adjacent subarrays, and $\beta = 2\pi/\lambda$ is the spatial wavenumber of the carrier frequency. $n(t)$ is the zero-mean white Gaussian noise with a variance of σ^2, which is shown as $n(t) \sim N(0, \sigma^2)$. For the 1-D DoA estimation, each subarray comprises elements modulated by a square wave $P_n(t)$.

$$P_n(t) = \begin{cases} 1, & NT_{pn} \le t < (N+\mu_n)T_{pn} \\ 0, & (N+\mu_n)T_{pn} \le t < (N+1)T_{pn} \end{cases} \tag{3}$$

In the formula, N is an integer, $T_{pn} = 1/f_{pn}$ is the modulation period of the nth column subarray, μ_n is duty ratio. We can rewrite $P_n(t)$ according to the Fourier series, as

$$P_n(t) = \sum_{q=-\infty}^{\infty} c_q^n e^{j2\pi q f_{pn} t} \tag{4}$$

$$c_q^n = \frac{1}{T_{pn}} \int_0^{T_{pn}} P_n(t) e^{-j2\pi q f_{pn} t} dt = \mu_n \mathrm{sinc}(\pi q \mu_n) e^{-j\pi q \mu_n}. \tag{5}$$

According to (5), $P_n(t)$ is influenced by the duty ratio μ_n and the order q. To simplify the analysis, we assume that the modulation function $P_n(t)$ shares the same duty ratio, in which case c_q^n can be abbreviated as c_q. Then, the Fourier transform of $P_n(t)$ can be expressed as

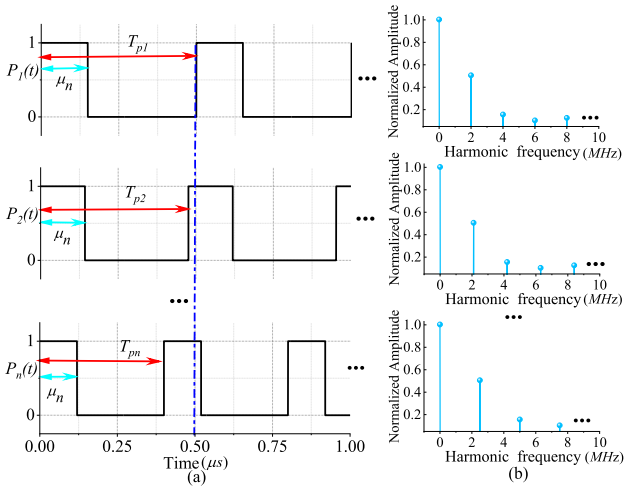

Fig. 2. Spatio-temporal modulation scheme. (a) Square waves with different modulation periods. (b) Fourier transform corresponding to the square wave.

$$P_n(f) = \mathcal{F}\{P_n(t)\} = \sum_{q=-\infty}^{\infty} c_q \delta(f - q f_{pn}). \tag{6}$$

In our work, different units are modulated at distinct frequencies. As shown in Fig. 2, the STMM generates harmonics based on different modulation schemes at various frequencies. We can prevent overlapping these harmonics by selecting an appropriate modulation frequency. Additionally, considering the amplitude-phase imbalance of the channel, the considering the amplitude-phase imbalance of the channel, the final signal model is expressed as follows:

$$\begin{aligned} y(t) &= \sum_{n=1}^{N} W_n P_n(t) s(t) e^{-j\beta(n-1)d\sin\theta} + n(t) \\ &= \sum_{n=1}^{N} \sum_{q=-\infty}^{\infty} W_n c_q e^{j2\pi q f_{pn} t} e^{j2\pi f_c t} e^{-j\beta(n-1)d\sin\theta} + n(t) \end{aligned} \tag{7}$$

$$W_n = \sum_{m=1}^{M} w_{mn} e^{-j\beta d_{mn}} \tag{8}$$

where W_n represents the magnitude and phase response between the nth subarray and the receiving horn antenna. Therefore, the received signal model can be written as

$$y_n(t) = S(t) W_n P_n(t) A_q + n. \tag{9}$$

It can be deduced from (7) that the output spectrum will contain frequency components $f = q f_{pn} + f_c$. The received single-channel signal can be expressed as follows:

$$\begin{aligned} y(f) &= \mathcal{F}\{y_n(t)\} = \sum_{n=1}^{N} W_n P_n(f) * s(f) A_q + n'(t) \\ &= \sum_{n=1}^{N} \sum_{q=-\infty}^{+\infty} W_n A_q \delta(f - q f_{pn} - f_c) + n'(t). \end{aligned} \tag{10}$$

It is important to note that the duty cycle and modulation period of the square-wave sequence shape the harmonic spectrum according to (4)–(6), while spatial phase delay across subarrays encodes incident angle information. Consequently, the relative

amplitude ratio and phase difference between the +1st and +2nd harmonics reflect both the intrinsic characteristics of the modulation pattern and a mapping to the DoA. For convenience, the +1st and +2nd can be rewritten as

$$y_{q=1}(f) = W_n P_1 S A_1 + n \tag{11}$$

$$y_{q=2}(f) = W_n P_2 S A_2 + n. \tag{12}$$

Mathematically, the matrix $y_{q=2}$ is quadratic in the matrix $y_{q=1}$. Then, $P1$ can be estimated by the relative phase difference between the +1st and +2nd harmonics, which is obtained by

$$\tilde{P}_1 = \arg[[y_{q=2}(f)]^* \odot y_{q=1}(f)]. \tag{13}$$

According to the conventional DoA estimation based on multiple-channel arrays, the received signals are defined as $\mathrm{X} = \mathrm{AS} + \mathrm{n}$, which is combined with multiple sources and noises. Thus, the procedure for restoring the single-channel signal can be articulated as

$$W_n{}^{-1} \tilde{P}_1^{-1} y_{q=1}(f) = S A_1 + n = \tilde{x}. \tag{14}$$

After recovering the array signals, the classic MUSIC algorithm is applied for spatial spectrum estimation. The novelty of this work lies not in the MUSIC algorithm itself, which is a well-known technique for spatial spectrum estimation.

B. Numerical and Experimental Validation

First, consider a metasurface consisting of 6×6 elements with a spacing of $\lambda/4$. The carrier frequency f_c of incident waves is 5 GHz. For 1-D estimation, the metasurface is divided into six subarrays, which are modulated by frequencies of 2.0 MHz to 2.5 MHz with a step of 0.1 MHz to distinguish the harmonics generated by different subarrays in the frequency spectrum. The modulated waves then focus on the receiving horn antenna and are synthesised into single-channel signals, which consist of many harmonic components generated by the time modulation.

Besides, the single-channel signals will be downconverted into a baseband signal. We use a sampling rate of 14 MHz to quantize them. There are A total number of 65 536 samples that are sampled to achieve angle estimation. Additionally, since only a few snapshots are needed for MUSIC, reducing the sampling size or using compressed sensing techniques can speed up DoA estimation [29], [30]. Meanwhile, real-time implementations on FPGA or GPU platforms are expected to further reduce latency [31]. Fig. 3(a) shows the normalized power spectrum of the simulated single-channel received signal in MATLAB. Fig. 3(b) and (c) shows the results of DoA estimation by the MUSIC algorithm. The spectral peak is observed at 30° for 1-D estimation and at (30°, 40°) for 2-D estimation. Fig. 3(d) shows the root-mean-square error (RMSE) of θ from 0° to 60° against signal-to-noise ratio (SNR). The RMSE significantly decreases as SNR increases from −20 dB to 10 dB. Fig. 4 illustrates the algorithm design and calculation process. Then, we simulated and fabricated a 6×6 STMM array to validate the algorithm's accuracy. Fig. 5(a) and (b) illustrates the top and bottom layers of the proposed metasurface, respectively. Fig. 5(c) shows the element's dimensions. The substrate is made of 1 mm-thick Rogers RT5880 material. The upper layer consists of metal strips with two integrated PIN diodes connected to the feed network on the rear side through holes. The practical circuits corresponding to different states are depicted in Fig. 5(d), where $R = 0.2\ \Omega$, L = 0.5 nH, and $C = 250$ pF. Fig. 5(e) illustrates the configuration for setting periodic boundary conditions for each unit cell. The specific geometrical parameters were defined as follows: P1 = 10 mm, P2 = 10 mm, $d = 15$ mm, $L_1 = 1$ mm, $W_1 = 0.5$ mm,

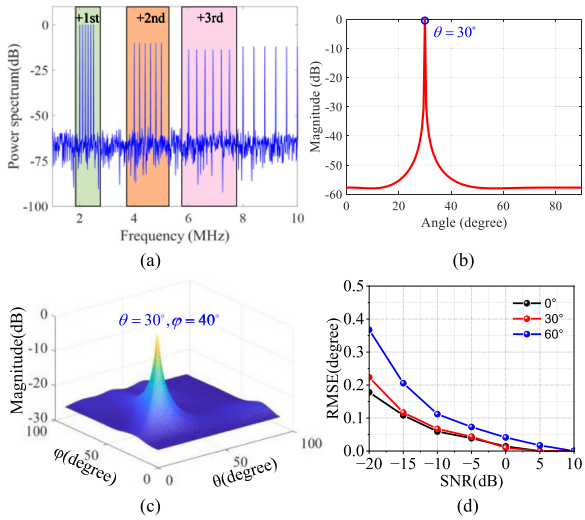

Fig. 3. (a) Normalized power spectrum. (b) 1-D and (c) 2-D DoA estimation results. (d) RMSE with different SNR.

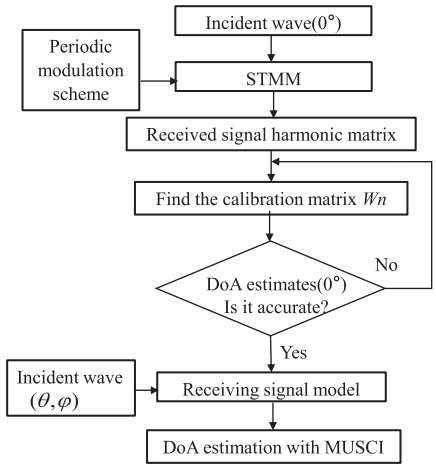

Fig. 4. Logical flow of STMM for DoA estimation.

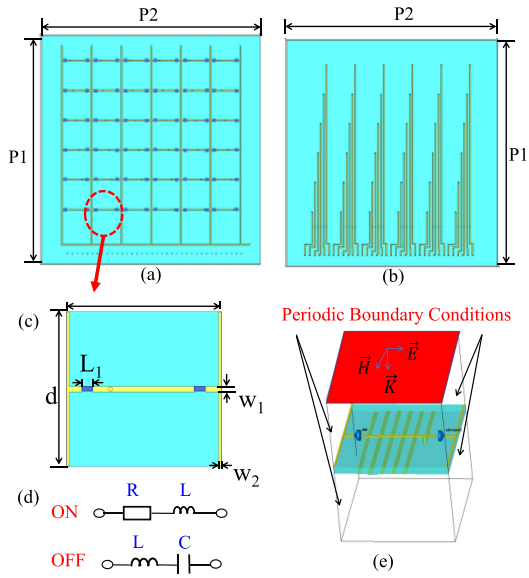

Fig. 5. Geometry of the metasurface array of (a) top layer and (b) bottom layer. (c) Unit cell. (d) Equivalent circuit of the diode. (e) Boundary conditions.

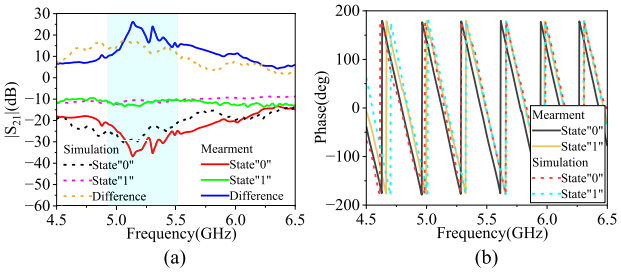

Fig. 6. Experiments and simulations of the transmission coefficients of the proposed STMM samples at different states. (a) Amplitude. (b) Phase.

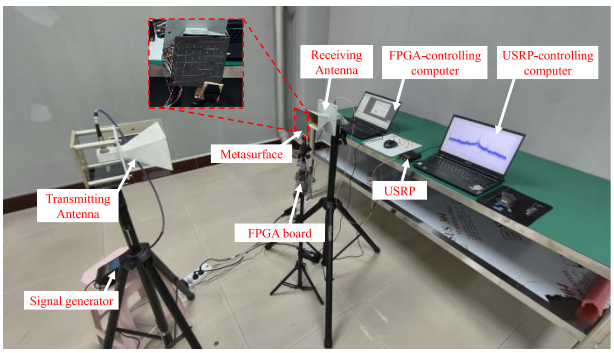

Fig. 7. Measurement environment for DoA estimation of the proposed STMM.

TABLE I
EMPIRICAL TESTING OF VARIOUS INCIDENT ANGLES

Incident angle	0°	10°	20°	30°	40°	50°	60°
RSME (deg)	0	0	0.15	0.20	0.31	0.46	0.61

$W_2 = 0.25$ mm. Fig. 6 compares the transmission amplitude and phase between simulations and experimental results for the PIN diode in "ON" and "OFF" states. In Fig. 6(a), when the diode is conducting, the S_{21} amplitude for the STMM is high, indicating a transmitted state. Conversely, in the OFF state, the amplitude significantly decreases to nearly negligible levels. The difference exceeds 10 dB within the 4.86 GHz to 5.51 GHz frequency range. Fig. 6(b) shows that both transmission coefficients have similar phase characteristics in this frequency band, indicating that the designed metasurface can adjust amplitude while maintaining a consistent phase at 5 GHz.

Furthermore, based on the working principle and process of the direction-finding system, an experimental platform was built as shown in Fig. 7. The EM waves emitted by the signal source at 5 GHz reach the surface of the STMM through the transmitting horn antenna. The experimental platform for the DoA estimate system is shown in Fig. 7. The metasurface is divided into six subarrays for one-dimensional DoA estimation, with parameters matching those in numerical simulations. Fig. 8(a) and (b) displays the normalized power spectra of received signals measured by the universal software radio peripheral (USRP) at incident angles of 0°, 30°, and 60°. Fig. 8(d) and (f) shows spatial spectra at different angles, spectral peaks accurately align with their respective directions, particularly pronounced along the normal direction.

Table I summarizes root mean square errors from fifty repeated angle measurements. The results indicate that the estimated angle error for 1-D DoA using the proposed STMM is below 0.61°. As summarized in Table II, most prior studies [21], [23], [26] have focused on phase modulation or reflective

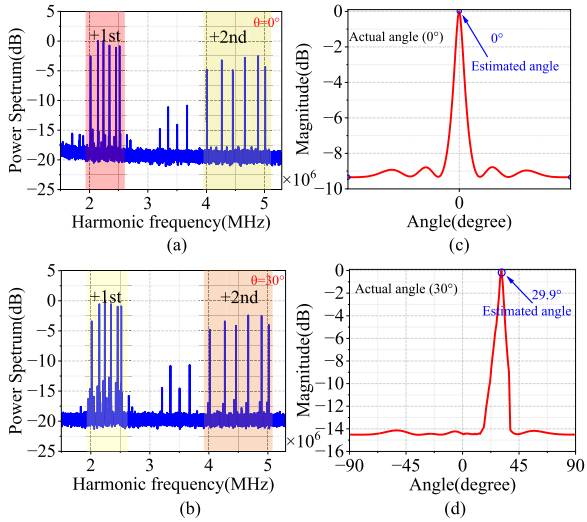

Fig. 8. Result of the experimental test. (a) and (b) Received signal spectrum. (c) and (d) DoA estimation result.

TABLE II
COMPARISON OF PROPOSED STMM WITH EXISTING METASURFACE FOR DOA ESTIMATE

Ref.	Unit	Array	Type of modulation	Transmission vs. reflection	RSEM (SNR>0 dB)
[21]	λ/2	20×20	Phase	Reflection	<2.5°
[23]	λ/2	32×24	Amplitude	Reflection	<1°
[26]	λ/2	20×20	Phase	Reflection	<1°
[28]	λ/2	6×6	Amplitude	Transmission	<0.31°
This work	**λ/4**	**6×6**	**Amplitude**	**Transmission**	**<0.15°**

metasurfaces. The amplitude-controlled transmissible metasurface in [28] incurs higher power consumption and costs due to amplifiers, resulting in a larger and heavier array. Our research shows that a simpler approach using nonuniform time-modulated amplitude control with subwavelength unit cells can be employed. This method achieves high precision while enabling a more compact, low-profile system with potentially lower power consumption.

III. CONCLUSION

This study proposes a transmissive amplitude-adjustable metasurface for single-channel DoA estimation. Unlike most phase-controllable metasurfaces, this direction-finding system ensures high accuracy in DoA estimation and features a low profile, compact size, and simple structure. A prototype of the metasurface composed of 6×6 components was fabricated. The maximum measurement error observed is 0.61°, demonstrating a high level of accuracy and compactness compared to the most advanced systems currently available. The proposed 1-bit adjustable amplitude STMM provides a compact and effective method for DoA estimation. However, the limitations of amplitude modulation restrict both effective radiation intensity and active beamforming capabilities. These tradeoffs highlight our design's current constraints but do not affect the accuracy of the single-channel DoA estimates in this study. Future research will explore hybrid amplitude-phase designs and integrated amplifiers to improve harmonic power, addressing these challenges.

REFERENCES

[1] J. Y. Dai et al., "Simultaneous in situ direction finding and field manipulation based on space-time-coding digital metasurface," *IEEE Trans. Antennas Propag.*, vol. 70, no. 6, pp. 4774–4783, Jun. 2022.

[2] A. Tennant and B. Chambers, "A two-element time-modulated array with direction-finding properties," *IEEE Antennas Wireless Propag. Lett.*, vol. 6, pp. 64–65, 2007.

[3] F. Belloni, A. Richter, and V. Koivunen, "DoA estimation via manifold separation for arbitrary array structures," *IEEE Trans. Signal Process.*, vol. 55, no. 10, pp. 4800–4810, Oct. 2007.

[4] C. Rai and D. Sen, "Low complexity DoA-ToA signature estimation for multi-antenna multi-carrier systems," in *Proc. IEEE Int. Conf. Acoust., Speech Signal Process.*, 2025, pp. 1–5.

[5] D. Inserra and A. M. Tonello, "A multiple antenna wireless testbed for the validation of DoA estimation algorithms," *AEU-Int. J. Electron. Commun.*, vol. 68, no. 1, pp. 10–18, 2014.

[6] T. Zhang et al., "Photonic-assisted multi-antenna frequency-spatial compressed sensing array for joint frequency and DOA estimation," *J. Lightw. Technol.*, vol. 42, no. 21, pp. 7678–7685, Nov. 2024.

[7] M. Gupta, S. Sharma, H. Joshi, and S. J. Darak, "Reconfigurable architecture for spatial sensing in wideband radio front-end," *IEEE Trans. Circuits Syst. II, Exp. Briefs*, vol. 69, no. 3, pp. 1054–1058, Mar. 2022.

[8] H. Tan, N. Xie, L. Huang, and H. Li, "Enhancing GNSS signal authentication through multi-antenna systems," *IEEE Trans. Wireless Commun.*, vol. 24, no. 5, pp. 4361–4376, May 2025.

[9] W. Kummer, A. Villeneuve, T. Fong, and F. Terrio, "Ultra-low sidelobes from time-modulated arrays," *IEEE Trans. Antennas Propag.*, vol. AP-11, no. 6, pp. 633–639, Nov. 1963.

[10] C. He, X. Liang, Z. Li, J. Geng, and R. Jin, "Direction finding by time-modulated array with harmonic characteristic analysis," *IEEE Antennas Wireless Propag. Lett.*, vol. 14, pp. 642–645, 2015.

[11] C. He et al., "Direction finding by time-modulated linear array," *IEEE Trans. Antennas Propag.*, vol. 66, no. 7, pp. 3642–3652, Jul. 2018.

[12] J. Chen et al., "Direction finding based on time-modulated array with multi harmonic analysis," *IEEE Trans. Antennas Propag.*, vol. 68, no. 7, pp. 5753–5758, Jul. 2020.

[13] J. Chen et al., "Direction finding of linear frequency modulation signal in time modulated array with pulse compression," *IEEE Trans. Antennas Propag.*, vol. 68, no. 1, pp. 509–520, Jan. 2020.

[14] Y. Yin et al., "Biquaternion-based DOA estimation of noncircular signals with time-modulated antenna arrays," *AEU-Int. J. Electron. Commun.*, vol. 159, 2023, Art. no. 154466.

[15] X. Jiang, G. Ni, A. Cao, C. Shao, and C. He, "Single-channel spatial spectrum estimation direction finding by the time-modulated linear array," *IEEE Antennas Wireless Propag. Lett.*, vol. 20, no. 12, pp. 2491–2495, Dec. 2021.

[16] W. Wu et al., "Time modulated array antennas: A review," *Electromagn. Sci.*, vol. 2, no. 1, pp. 1–19, 2024.

[17] Y. Man et al., "An efficient multi-beamforming method based on 1-bit phase modulation for time-modulated arrays," *IEEE Trans. Antennas Propag.*, vol. 73, no. 6, pp. 3654–3665, Jun. 2025.

[18] B. Zheng, J. Zhang, Y. Shan, N. Li, and Y. Zhang, "Wideband RCS reduction metasurface based on printing resistive graphene ink," *IEEE Antennas Wireless Propag. Lett.*, vol. 23, no. 7, pp. 2041–2045, Jul. 2024.

[19] G. B. Wu et al., "A synthetic moving-envelope metasurface antenna for independent control of arbitrary harmonic orders," *Nature Commun.*, vol. 15, no. 1, 2024, Art. no. 7202.

[20] M. Wang, D. Liao, J. Y. Dai, and C. H. Chan, "Dual-polarized reconfigurable metasurface for multifunctional control of electromagnetic waves," *IEEE Trans. Antennas Propag.*, vol. 70, no. 6, pp. 4539–4548, Jun. 2022.

[21] L. Bai, H. Cao, T. Bai, and C. He, "1-bit programmable metasurface-based 2-D direction finding," *IEEE Antennas Wireless Propag. Lett.*, vol. 22, no. 9, pp. 2160–2164, Sep. 2023.

[22] W. Li, N. Wang, and J. Qi, "Direct angle of arrival (AOA) estimation using a metasurface antenna with single frequency phaseless measurements obeyed Schwarz inequality," *IEEE Trans. Microw. Theory Techn.*, vol. 72, no. 4, pp. 2677–2685, Apr. 2024.

[23] X. Fang et al., "Multifunctional space–time-modulated metasurface for direction of arrival estimation and RCS manipulation in a single system," *IEEE Trans. Microw. Theory Techn.*, vol. 72, no. 6, pp. 3797–3808, Jun. 2024.

[24] J. An et al., "Two-dimensional direction-of-arrival estimation using stacked intelligent metasurfaces," *IEEE J. Sel. Areas Commun.*, vol. 42, no. 10, pp. 2786–2802, Oct. 2024.

[25] M. Lin et al., "Single sensor to estimate DOA with programmable metasurface," *IEEE Internet Things J.*, vol. 8, no. 12, pp. 10187–10197, Jun. 2021.

[26] W. Wang et al., "High-precision direction-of-arrival estimations using digital programmable metasurface," *Adv. Intell. Syst.*, vol. 4, no. 4, 2022, Art. no. 2100164.

[27] Q. Y. Zhou et al., "Two-dimensional direction-of-arrival estimation based on time-domain-coding digital metasurface," *Appl. Phys. Lett.*, vol. 121, no. 18, 2022.

[28] D. Xia et al., "Accurate 2-D DoA estimation based on active metasurface with nonuniformly periodic time modulation," *IEEE Trans. Microw. Theory Techn.*, vol. 71, no. 8, pp. 3424–3435, Aug. 2023.

[29] J. Cao, Z. Yang, M. Xiao, X. Chen, and A. K. Nandi, "Delay coprime array: A new sparse linear array for fast and robust DoA estimation," *IEEE Signal Process. Lett.*, vol. 32, pp. 3994–3998, 2025.

[30] J. I. Yameng et al., "Maximum likelihood DoA estimation based on improved ant colony optimization algorithm," *J. Shenzhen Univ. Sci. Eng.*, vol. 40, no. 1, 2023.

[31] Q. Huang and N. Lu, "Optimized real-time MUSIC algorithm with CPU-GPU architecture," *IEEE Access*, vol. 9, pp. 54067–54077, 2021.